arXiv:astro-ph/0212310v2 5 Aug 2003

Gravitational Lensing by a Compound Population of Halos: Standard Models

Li-Xin Li[a,1] and Jeremiah P. Ostriker[b]

[a] *Harvard-Smithsonian Center for Astrophysics, Cambridge, MA 02138, USA*

lli@cfa.harvard.edu

[b] *Institute of Astronomy, University of Cambridge, Madingley Road, Cambridge CB3 0HA, UK*

jpo@ast.cam.ac.uk

ABSTRACT

Based on observed rotation curves of galaxies and theoretical simulations of dark matter halos, there are reasons for believing that at least three different types of dark matter halos exist in the Universe classified by their masses M and the inner slope of mass density $-\alpha$: Population A (galaxies): $10^{10}h^{-1}M_\odot \lesssim M \lesssim 2\times10^{13}h^{-1}M_\odot$, $\alpha\approx 2$; Population B (cluster halos): $M \gtrsim 2\times10^{13}h^{-1}M_\odot$, $\alpha \approx 1.3$; and Population C (dwarf halos): $M \lesssim 10^{10}h^{-1}M_\odot$, $\alpha \approx 1.3$. In this paper we calculate the lensing probability produced by such a compound population of dark halos, for both image separation and time delay, assuming that the mass function of halos is given by the Press-Schechter function and the Universe is described by an LCDM, OCDM, or SCDM model. The LCDM model is normalized to the *WMAP* observations, OCDM and SCDM models are normalized to the abundance of rich clusters. We compare the predictions of the different cosmological models with observational data and show that, both LCDM and OCDM models are marginally consistent with the current available data, but the SCDM model is ruled out. The fit of the compound model to the observed correlation between splitting angle and time delay is excellent but the fit to the number vs splitting angle relation is only adequate using the small number of sources in the objective JVAS/CLASS survey. A larger survey of the same type would have great power in discriminating among cosmological models. Furthermore, population C in an LCDM model has a unique signature

[1] Chandra Fellow

in the time domain, an additional peak at ~ 3 seconds potentially observable in GRBs, which makes it distinguishable from variants of CDM scenarios, such as warm dark matter, repulsive dark matter, or collisional dark matter. For image separations greater than 10 arcseconds the differently normalized LCDM models predict significantly different lensing probabilities affording an additional lever to break the degeneracies in the CMB determination of cosmological parameters.

Subject headings: cosmology: gravitational lensing — galaxies: clusters: general — galaxies: halos

1. Introduction

It is well known that gravitational lensing is a powerful tool for directly probing the structure and distribution of dark matter in the Universe (Turner, Ostriker, & Gott 1984; Schneider, Ehlers, & Falco 1992; Bartelmann & Schneider 2001; Courbin, Saha, & Schechter 2002, and references therein). By comparing the number of lenses found in a survey of remote sources (e.g., quasars, radio galaxies, or high redshift type Ia supernova) to theoretical predictions, we should be able to deduce the quantity of dark matter in the Universe and how it is distributed (Turner 1990; Wambsganss et al. 1995; Porciani & Madau 2000; Keeton 2001; Keeton & Madau 2001; Li & Ostriker 2002, henceforth LO02; Gladders et al. 2003). The joint observations of gravitational lensing, high redshift type Ia supernova, cosmic microwave background (CMB), and cluster abundances constrain the Universe to be in all likelihood flat and accelerating, with the present mass density being composed of about 70% cosmological constant (or dark energy), 26% dark matter, and 4% ordinary matter (Ostriker & Steinhardt 1995; Bahcall et al. 1999; Wang et al. 2000; Peacock et al. 2001; Efstathiou et al. 2002; Yamamoto 2002; Spergel et al. 2003).

However, the lensing cross-section (and thus the lensing probability) is found to be extremely sensitive to the inner density profile of lenses (Keeton & Madau 2001; Wyithe, Turner, & Spergel 2001; LO02). For example, with fixed total mass, when the inner slope of the density profile, $-\alpha$, changes from -1 [the NFW case (Navarro, Frenk, & White 1996, 1997)] to -2 [the singular isothermal sphere (SIS) case (Gott & Gunn 1974; Turner, Ostriker, & Gott 1984)] while maintaining the same mass density in lenses, the integral lensing probability increases by more than two orders of magnitudes for the flat model of the Universe (LO02). Therefore, lensing also sensitively probes small scale structure. This complicates matters and renders it is hazardous to use observed lensing statistics to draw inferences with regard to cosmology before determining the sensitivity to other factors.

In LO02, we have shown that in order to explain the observed numbers of lenses found in the JVAS/CLASS survey, at least two populations of dark halos must exist in nature. One population, which corresponds to normal galaxies, has masses $\lesssim 10^{13} M_\odot$ and a steep inner density profile ($\alpha \approx 2$, i.e. SIS) presumably determined by the distribution of baryonic material in the inner parts of galaxies;[2] the other one, which corresponds to groups or clusters of galaxies, has masses $\gtrsim 10^{13} M_\odot$ and a shallow inner density profile ($\alpha \lesssim 1.4$, i.e. similar to NFW). A similar conclusion has been obtained by Porciani & Madau (2000) for explaining the number of lenses found in the CASTLES survey. These results are consistent with the theoretical studies on the cooling of massive gas clouds: there is a critical mass of halos $\sim 10^{13} M_\odot$ below which cooling of the corresponding baryonic component will lead to concentration of the baryons to the inner parts of the mass profile (Rees & Ostriker 1977; Blumenthal et al. 1986).

In this paper we investigate the lensing statistics produced by a compound population of halos. We assume that there are three populations of halos in the Universe:

— Population A: $10^{10} h^{-1} M_\odot < M < 2 \times 10^{13} h^{-1} M_\odot$, $\alpha = 2$ (SIS);
— Population B: $M > 2 \times 10^{13} h^{-1} M_\odot$, $\alpha = 1.3$ [GNFW (generalized NFW, Zhao 1996)];
— Population C: $M < 10^{10} h^{-1} M_\odot$, $\alpha = 1.3$ (GNFW),

where h is the Hubble constant in units of 100 km s^{-1} Mpc^{-1}. Population A corresponds to spiral and elliptical galaxies, whose centers are dominated by baryonic matter. Population B corresponds to groups or clusters of galaxies, whose centers are dominated by dark matter. Population C corresponds to dwarf galaxies or subgalactic objects, whose centers lack baryons due to feedback processes such as supernova explosions, stellar winds, and photoionizations (Kauffmann, White, & Guiderdoni 1993; Somerville & Primack 1999; Benson et al. 2002; Ma 2003), and so are also dominated by dark matter. We adopt an inner slope for the dark matter halos of $\alpha = 1.3$ consistent with the value 1.3 ± 0.2 found by Subramanian, Cen, & Ostriker (2000) and intermediate between the values advocated by Navarro, Frenk, & White (1996, 1997) of $\alpha = 1.0$ and Ghigna et al. (2000) of $\alpha = 1.5$. We will calculate here the lensing probability of two measurable variables: image separation and time delay, examining in a subsequent paper the expected arc properties.

Recently, Davis, Huterer, & Krauss (2003) used lensing statistics to constrain the inner slope of lensing galaxies. Using the Schechter function (Schechter 1976), they constrained

[2]Strictly speaking, the mass density profile of galaxies is the combination of the density profile of hark halos and that of baryonic material at the centers. For brevity, in the paper we still call it the mass density of halos, though we mean the sum of the mass density of dark halos and that of baryonic material whenever we refer to galaxies.

the inner slope of lensing galaxies to the range from 1.58 to 1.98, at 95% confidence level (CL). It is hard to predict how their result would change if the Press-Schechter function (Press & Schechter 1974) were used. Our choice of $\alpha = 2$ for galaxies is supported by the following fact: stellar dynamics of elliptical galaxies, modeling of lensed systems, and flux ratios of multiple images all give an inner profile that is consistent with SIS (Rix et al. 1997; Romanowsky & Kochanek 1999; Cohn et al. 2001; Rusin & Ma 2001; Treu & Koopmans 2002; Rusin 2002; Rusin, Kochanek, & Keeton 2003).

Sand, Treu, & Ellis (2002) have reported a remarkably flat inner slope in the lensing cluster MS2137-23: $\alpha < 0.9$ at 99% CL. However, by measuring the average gravitational shear profile of six massive clusters of virial masses $\sim 10^{15} M_{\odot}$, Dahle, Hannestad, & Sommer-Larsen (2003) have found that the data are well fitted by a mass density profile with $\alpha \sim 0.9 - 1.6$ for SCDM model and $\alpha \sim 1.3 - 1.6$ for LCDM model, both at 68% CL. So, our choice of $\alpha = 1.3$ for population B looks reasonable. The inner density slopes for small mass halos are not well constrained. CDM simulations generally predict a cusped inner density, while other dark matter models, like warm dark matter (Bode, Ostriker, & Turok 2001), repulsive dark matter (Goodman 2000), and collisional dark matter (Spergel & Steinhard 2000), tend to predict flatter inner density (see also Ricotti 2002). Our choice of $\alpha = 1.3$ for population C should be a reasonable upper limit. In her recent paper, by requiring that the Schechter luminosity function and the Press-Schechter mass function to give consistent predictions for the image separation below $1''$, Ma (2003) has shown that the fraction of SIS halos peaks around mass of $10^{12} M_{\odot}$ and quickly drops for large and small mass halos. This is qualitatively consistent with the model that we adopt in this paper.

The paper is organized as follows: In §2 we write down the lensing cross-section produced by SIS and GNFW halos. In §3 we show how to calculate the lensing probability, assuming that halos are composed of the population defined above, whose mass function is given by the Press-Schechter function (Press & Schechter 1974). In §4 we present our results. In §5 we summarize and discuss our results.

2. Lensing by SIS and GNFW Halos

Issues related to image separation are presented in LO02 in detail, so here we focus on the time delay between multiple images produced by gravitational lensing.

2.1. Singular isothermal sphere

The density profile for an SIS is (Gott & Gunn 1974; Turner, Ostriker, & Gott 1984)

$$\rho(r) = \frac{\sigma_v^2}{2\pi G}\frac{1}{r^2} \,, \tag{1}$$

where σ_v is the constant velocity dispersion.

Assuming that the angular-diameter distances from the observer to the lens and the source are respectively D_L^A and D_S^A, from the lens to the source is D_{LS}^A. Then, the time delay between the two images of the remote source lensed by an SIS halo is (Schneider, Ehlers, & Falco 1992)

$$\Delta t = \Delta t_1 \, y \,, \qquad \Delta t_1 \equiv \frac{8\pi\xi_0}{c}\left(\frac{\sigma_v}{c}\right)^2 (1+z_L) \,, \tag{2}$$

where

$$\xi_0 \equiv 4\pi\left(\frac{\sigma_v}{c}\right)^2 D_R^A \,, \qquad D_R^A \equiv \frac{D_L^A D_{LS}^A}{D_S^A} \,, \tag{3}$$

z_L is the redshift of the lens (dark halo), y is the distance from the source to the point where the line of sight through the lens center intersects the source plane, in units of $\eta_0 \equiv \xi_0 D_S^A / D_L^A$.

The cross-section for producing two images with a time delay $> \Delta t$ is

$$\sigma(>\Delta t) = \pi\xi_0^2\left[1 - \left(\frac{\Delta t}{\Delta t_1}\right)^2\right] \vartheta(\Delta t_1 - \Delta t) \,, \tag{4}$$

where $\vartheta(\Delta t_1 - \Delta t)$ is the step function.

2.2. Generalized NFW profile

The density profile for a GNFW profile is (Zhao 1996; Wyithe, Turner, & Spergel 2001; LO02)

$$\rho(r) = \frac{\rho_s r_s^3}{r^\alpha (r+r_s)^{3-\alpha}} \,, \tag{5}$$

where α, ρ_s, and r_s are constants. The case of $\alpha = 1$ corresponds to the NFW profile (Navarro, Frenk, & White 1996, 1997). The case of $\alpha = 2$, $r_s \to \infty$ but keeping $\rho_s r_s^2$ constant, corresponds to the SIS profile. In this paper, we take $\alpha = 1.3$ for Populations B and C.

In the lens plane, we denote the distance from the lens center to the point where the light ray of the source object intersects the lens plane by x, in units of r_s. In the source plane, we denote the distance from the source to the point where the line of sight through the lens center intersects the source plane by y, in units of $r_s D_S^A/D_L^A$. Then, the lensing equation is (LO02)

$$y = x - \mu_s \frac{g(x)}{x} , \qquad g(x) \equiv \int_0^x u du \int_0^\infty dz (u^2+z^2)^{-\alpha/2} \left[(u^2+z^2)^{1/2}+1\right]^{\alpha-3} , \tag{6}$$

where

$$\mu_s \equiv \frac{16\pi G}{c^2} \rho_s r_s D_R^A . \tag{7}$$

To a good approximation, the time delay between the two images produced by a GNFW halo is given by (Oguri et al. 2002)

$$\Delta t \approx \Delta t_2 \frac{y}{y_r} , \qquad \Delta t_2 \equiv \frac{2 r_s^2 x_t}{c D_R^A} (1+z_L) y_r , \tag{8}$$

where x_t is the positive root of $y(x) = 0$, y_r corresponds to the positive y at $dy/dx = 0$.

The cross-section for producing two images with a time delay $> \Delta t$ is

$$\sigma(>\Delta t) = \pi y_r^2 r_s^2 \left[1 - \left(\frac{\Delta t}{\Delta t_2}\right)^2\right] \vartheta(\Delta t_2 - \Delta t) . \tag{9}$$

3. Gravitational Lensing Produced by the Compound Population

The probability for a remote point source lensed by foreground dark halos is given by

$$P = 1 - e^{-\tau} , \qquad \tau \equiv \int_0^{z_S} dz_L \frac{dD_L}{dz_L} \int_0^\infty dM\, n(M, z_L) \sigma(M, z_L) , \tag{10}$$

where z_S is the redshift of the source, D_L is the proper distance from the observer to a lens at redshift z_L, $n(M, z_L)dM$ is the proper number density of lens objects of masses between M and $M + dM$, $\sigma(M, z_L)$ is the lensing cross-section of a dark halo of mass M at redshift z_L. When $\tau \ll 1$ (which is true in most cases for lensing statistics), we have $P \approx \tau$.

For both SIS and GNFW profiles, the mass contained within radius r diverges as $r \to \infty$. So, a cutoff in radius must be introduced. Here, as is typically done in the literature, we define the mass of a dark halo to be the mass within a sphere of radius $r = r_{200}$, where r_{200}

is the radius within which the average mass density is 200 times the critical mass density of the universe at the redshift of the halo.

As in LO02, we consider three kinds of cosmological models: LCDM, OCDM, and SCDM. We assume that the number density of dark halos is distributed in mass according to the Press-Schechter function (Press & Schechter 1974). We compute the CDM power spectrum using the fitting formula given by Eisenstein & Hu (1999), where, to be consistent with the recent observations of *WMAP* (Spergel et al. 2003), we assume the Hubble constant $h = 0.7$ and the primordial spectrum index $n_s = 0.96$. For OCDM and SCDM, we determine the value of σ_8 by the cluster abundances constraint (Wang & Steinhardt 1998; Wang et al. 2000)

$$\sigma_8 \Omega_m^\gamma \approx 0.5 \, , \tag{11}$$

where $\gamma \approx 0.33 + 0.35\Omega_m$. For LCDM, we take Ω_m and σ_8 to be consistent with the observations of *WMAP* (Spergel et al. 2003): $\Omega_m = 0.27$ (then $\Omega_L = 0.73$), $\sigma_8 = 0.84$.

A new cluster abundances constraint has recently been obtained by Bahcall et al. (2003) with the SDSS data. The best-fit cluster normalization is given by $\sigma_8 \Omega_m^{0.6} = 0.33 \pm 0.03$ (for $0.1 \lesssim \Omega_m \lesssim 0.4$) for the flat model of the Universe with a Hubble constant $h = 0.72$. Bahcall et al. (2003) found that the best-fit parameters of the observed mass function are $\Omega_m = 0.19 \pm^{0.08}_{0.07}$ and $\sigma_8 = 0.9 \pm^{0.3}_{0.2}$. Recent calibration of the cluster data based on X-ray observations (Borgani et al. 2001; Reiprich & Böhringer 2002; Seljak 2002; Viana, Nichol, & Liddle 2002) are closer to the Bahcall et al. (2003) result. So, for comparison, we will also present some results for a flat LCDM model with the Bahcall et al. normalization to show the sensitivity of results to normalization.

For the case of image separation, the cross-section σ can be found in LO02 (eqs. [37] for SIS and [48] for GNFW). For the case of time delay, the cross-section is given by equation (4) for SIS halos, and equation (9) for GNFW halos.

We normalize the GNFW profile so that the concentration parameter $c_1 \equiv r_{200}/r_s$ satisfies (Oguri, Taruya, & Suto 2001; Oguri et al. 2002)

$$c_1(M, z_L) = c_{\rm norm} \frac{2-\alpha}{1+z_L} \left(\frac{M}{10^{14} h^{-1} M_\odot} \right)^{-0.13} \, . \tag{12}$$

Throughout the paper we fix $c_{\rm norm} = 8$, in consistence with the simulations (Bullock et al. 2001).

For the model of compound halo population considered in this paper, the integration over mass M is divided into three parts: $\int_0^{M_a}$ for GNFW with $\alpha = 1.3$, $\int_{M_a}^{M_b}$ for SIS, and $\int_{M_b}^{\infty}$ for GNFW with $\alpha = 1.3$; where $M_a = 10^{10} h^{-1} M_\odot$, $M_b = 2 \times 10^{13} h^{-1} M_\odot$.

4. Results

With the formalism described above, we are ready to calculate the lensing probability for images separation and time delay. The models to be calculated are listed in Table 1. As explained in the previous section, we take three different normalizations for LCDM models: in most of calculations we choose parameters to be consistent with *WMAP* (Spergel et al. 2003), but, for comparison, we will also present some results corresponding to the normalization of Bahcall et al. (2003). For OCDM and SCDM models, we adopt equation (11) for normalization. Throughout the paper we take $h = 0.7$ and $n_s = 0.96$.

4.1. Image separation

For image separation, we have calculated the differential lensing probability

$$\frac{dP}{d\lg\Delta\theta} \equiv -\frac{dP(>\Delta\theta)}{d\lg\Delta\theta}\ , \tag{13}$$

where $P(>\Delta\theta)$ is given by equation (10) with $\sigma = \sigma(>\Delta\theta)$. We show the results for different cosmological models in Figure 1, separately for the three different components in the whole population: Population A (galaxies, the highest island), Population B (groups and clusters of galaxies, the second high island), and Population C (dwarf galaxies and subgalactic objects, the lowest island). The source object is assumed to be at $z_S = 3$.

From the figure we see that, Population A (galaxies) contributes most to the total number of lenses, due to its steep inner density slope ($\alpha = 2$); Population B contributes less; Population C contributes least, due to its small mass and shallow inner density slope ($\alpha = 1.3$). Consistent with the results in LO02, the lensing probability produced by the $\alpha = 1.3$ GNFW halos is smaller than the lensing probability produced by SIS halos by two orders of magnitudes in the overlap regions. (The results here are slightly different from those in LO02 due to the fact that in this paper we use a different normalization in the concentration parameter, i.e. eq. [12].)

In Figure 2, we show the LCDM ($\Omega_m = 0.27$, $\sigma_8 = 0.84$) results corresponding to different redshift of the source object: from $z_S = 1$ to $z_S = 10$. We see that the lensing probability increases quickly with the source redshift, increasing by an order of magnitude between $z_S = 1$ and $z_S = 3$ (cf. Wambsganss, Bode, & Ostriker 2003). However, the rate of increase in the lensing probability decreases with the source redshift, this is because that the proper distance from the source object to the observer approaches a finite limit as $z_S \to \infty$ (due to the existence of a horizon in an expanding universe). We also see that, as the source redshift increases, the splitting angle corresponding to the peak probability of each

island shifts toward larger values. In Figure 3, we show the corresponding integral lensing probability

$$P(<\Delta\theta) = P(>0) - P(>\Delta\theta) \ . \tag{14}$$

To compare the predictions with observations, the effect of magnification bias must be considered (Turner, Ostriker, & Gott 1984; Schneider, Ehlers, & Falco 1992; LO02; Oguri et al. 2002). When the source objects have a flux distribution $\propto f^{-\beta}$ ($\beta < 3$) and the probability density for magnification is $\propto A^{-3}$, the magnification bias is given by (LO02)

$$B = \frac{2}{3-\beta} A_m^{\beta-1} \ , \tag{15}$$

where A_m is the minimum of the total amplification. For SIS lenses we have $A_m = 2$. For GNFW lenses, A_m can be approximated by

$$A_m \approx \frac{2x_t}{y_r y_t'} \ , \tag{16}$$

where $y_t' \equiv (dy/dx)(x = x_t)$.

Equation (16) is an improvement to the equation (68) of LO02. The magnification bias calculated with equations (15) and (16) agrees with that calculated with the more complicated formula of Oguri et al. (2002) with errors $< 5\%$ for $0.01 < \mu_s < 10$.

For GNFW lenses with $\alpha = 1.3$, we show the average magnification bias $\langle B \rangle$ (defined by the ratio of the biased lensing probability to that without bias) as a function of image separation in Figure 4 (as an improvement to the Fig. 10 of LO02) for the JVAS/CLASS survey (Meyers et al. 2003; Browne et al. 2003), where we have assumed $\beta = 2.1$ (Rusin & Tegmark 2001) and $z_S = 1.27$ (Marlow et al. 2000). The magnification bias for GNFW lenses depends on cosmological models, decreases with increasing image separation, and is bigger than the magnification bias for SIS lenses (which is a constant $B \approx 4.76$) by about 1.2 order of magnitude on average (for $\alpha = 1.3$).

In Figure 5, we compare our predictions (including magnification bias) for the compound model with observations from the JVAS/CLASS survey. The data are updated compared to Helbig (2000). The new data contain 13 lenses found in a sample of 8958 of radio sources which form a statistical sample (Browne et al. 2003). Considering error bars, both LCDM and OCDM models with both normalizations are marginally consistent with the JVAS/CLASS observational data.[3] Comparing LCDM2 with LCDM3, we find that even for the same cluster

[3]The apparent excess in the prediction for small splitting angles is caused by the angular selection effect: the JVAS/CLASS survey is limited to image separation $\geq 0.3''$ (Browne et al. 2003).

normalization there is significant discriminatory power available from lensing statistics (if data is available) in breaking the degeneracy on the $(\Omega_{\rm m}, \sigma_8)$ plane. This is consistent with our previous results (LO02). The three different LCDM models do not differ significantly in their predictions at small splittings but for splittings above 10 arcseconds the Bahcall et al normalization, LCDM3, predicts few lenses by more than a factor of five.

4.2. Time delay

For time delay, we have calculated the differential lensing probability

$$\frac{dP}{d\lg\Delta t} \equiv -\frac{dP(>\Delta t)}{d\lg\Delta t} \ , \tag{17}$$

where $P(>\Delta t)$ is given by equation (10) with $\sigma = \sigma(>\Delta t)$. We show the results in Figure 6, for the same models in §4.1.

We see that, the distribution of lensing probability over time delay is very similar to the distribution over image separation (compare Fig. 2 to Fig. 1). Again, the contribution to lensing events is overwhelmingly dominated by Population A due to its steep inner density slope. Population C contributes the least.

We have also calculated the lensing probability for time delay corresponding to different source redshift: from $z_S = 1$ to $z_S = 10$. The results for the LCDM model ($\Omega_m = 0.27$, $\sigma_8 = 0.84$) are shown in Figure 7 for the differential lensing probability $dP/d\lg\Delta t$, and Figure 8 for the integral lensing probability

$$P(<\Delta t) = P(>0) - P(>\Delta t) \ . \tag{18}$$

From these figures we see that, like in the case for image separation, the lensing probability sensitively depends on z_S for small z_S. For large z_S, the lensing probability becomes less sensitive to the source redshift, due to the fact that dD_S/dz_S decreases with increasing z_S.

We can calculate the joint lensing probability $P(>\Delta\theta, >\Delta t)$ by using the joint cross-section

$$\sigma(>\Delta\theta, >\Delta t) = \sigma(>\Delta\theta)\,\vartheta(\Delta t_i - \Delta t) \ , \tag{19}$$

where $\Delta t_i = \Delta t_1$ for SIS and Δt_2 for GNFW. The cross-section $\sigma(>\Delta\theta)$ is given by equation (37) of LO02 for SIS, and equation (48) of LO02 for GNFW. Then, we can calculate the conditional lensing probability $P(\Delta\theta, >\Delta t)$ defined by

$$P(\Delta\theta, >\Delta t) \equiv -\frac{\partial}{\partial\Delta\theta} P(>\Delta\theta, >\Delta t) \ , \tag{20}$$

which gives the distribution of lensing events over time delay for a given image separation.

Knowing $P(\Delta\theta, > \Delta t)$, we can calculate the median time delay $\Delta t_{\rm med}$ as a function of $\Delta\theta$, where $\Delta t_{\rm med}$ is defined by

$$P(\Delta\theta, > \Delta t_{\rm med}) = \frac{1}{2} P(\Delta\theta, > 0) \; . \tag{21}$$

The prediction for $\Delta t_{\rm med}$ as a function of $\Delta\theta$ is not sensitive to the magnification bias since it is determined by the ratio of two probabilities. So, the correlation between $\Delta t_{\rm med}$ and $\Delta\theta$ provides a test of lensing models independent of the determination of magnification bias.

The results of $\Delta t_{\rm med}(\Delta\theta)$ for the LCDM ($\Omega_m = 0.27$, $\sigma_8 = 0.84$; indeed the results are insensitive to the cosmological parameters) model are shown in Figure 9, where the source object is again assumed to be at $z_S = 1.27$. In Figure 9 we also show the quadrant deviations (dashed lines), which are defined by equation (21) with the 1/2 on the right-hand side being replaced by 1/4 and 3/4, respectively. The observational data, taken from Oguri et al. (2002), fit the LCDM model well. Comparison of Figure 9 with Oguri et al. (2002)'s Figure 6 indicates that our compound model fits the observations better. The single population model predicts a single (almost) straight line in the $\lg\Delta\theta - \lg\Delta t_{\rm med}$ space. For the compound model, a "step" is produced at the point where the mass density profile changes. The "step" that we see in Figure 9 corresponds to the transition from population A (galaxies) to population B (galaxy groups/clusters).

5. Summary and Discussion

As an extension of our previous work (LO02), we computed the lensing probability produced by a compound population of dark halos. We have calculated the lensing probability for both image separation and time delay. The calculations confirm our previous results (LO02) that the lensing probability produced by GNFW halos with $\alpha \lesssim 1.3$ is lower than that produced by SIS halos with same masses by orders of magnitudes, where $-\alpha$ is the inner slope of the halo mass density. So, for the compound population of halos, both the number of lenses with large image separation ($\Delta\theta \gtrsim 5''$) and the number of lenses with small image separation ($\Delta\theta \lesssim 10^{-2\,''}$) are greatly suppressed. The same conclusion holds also for the number of lenses with large time delay ($\Delta t \gtrsim 10\,$years) and the number of lenses with small time delay ($\Delta t \lesssim 10^{-4}\,$year). (See Figs. 1 and 6. This conclusion holds even when the effect of magnification bias is considered, see Figs. 4 and 5.)

We have also tested the dependence of the lensing probability on the redshift of the source object (Figs. 2, 3, 7, and 8). The results show that, the lensing probability is quite

sensitive to the change in the redshift of the source object. The number of lenses significantly increases as the source redshift increases. However, the rate of the increase decreases as the source redshift becomes large, which is caused by the fact that the proper cosmological distance approaches a finite limit when $z_S \to \infty$. Another interesting result is that, the peak of the lensing probability for each population moves toward large image separation or time delay, as the source redshift increases.

We see that population C (dwarf halos) in an LCDM model has a unique signature in the time domain, c.f. Figures 6 and 7. Time delays of less than 10 seconds and greater than 0.1 second are predicted and should be found in gamma-ray burst sources which are at cosmological distances and have the requisite temporal substructure. Variants of CDM, such as warm dark matter (Bode, Ostriker, & Turok 2001), repulsive dark matter (Goodman 2000), or collisional dark matter (Spergel & Steinhard 2000) would not produce this feature. However, current surveys do not go deep enough to provide a sufficiently large sample to test the prediction. When more observational data on gamma-ray burst time delay and small splitting angles become available, our calculations can be used to distinguish different dark matter models (Nemiroff et al. 2001; Wilkinson et al. 2001).

We have compared the distribution of the number of lenses over image separation predicted by our model with the updated JVAS/CLASS observational data, with the new *WMAP* cosmological parameters (Fig. 5). Since the JVAS/CLASS survey is limited to image separation $\geq 0.3''$ (Browne et al. 2003), we cannot test our predictions for small image separations. However, in the range that is probed by JVAS/CLASS, we see that both the LCDM and OCDM models fit the observation reasonably well and current data do not allow us to distinguish between the two proposed normalizations for the LCDM spectrum, even though these produce predictions that differ by a factor of roughly 1.4. An explicit search for lenses with image separation between $6''$ and $15''$ has found no lenses (Phillips et al. 2001), which rules out the SIS model for image separation in this range (LO02). This together with our Figure 5 supports our model of compound population of halos. For separations greater than $10''$ the differently normalized LCDM models produce significantly different results, thus producing an additional lever to break the degeneracies in the WMAP results (cf. Bridle et al. 2003)

We have also calculated the distribution of the mean time delay vs image separation for the LCDM model (Fig. 9). We see that, the compound model fits observations quite well, better than the model of single population of halos (Oguri et al. 2002). The compound model predicts a unique feature in the $\lg \Delta\theta - \lg \Delta t_{\rm med}$ plane: there is a "step" corresponding to the transition in mass density profile. This can be better tested when more observation data are available.

A controlled survey of lenses with double the sample size of CLASS, perhaps obtainable via SDSS (York et al. 2000; Stoughton et al. 2002), should allow one to better distinguish between LCDM variants and perhaps between LCDM models and those based on quintessence (Caldwell, Dave, & Steinhardt 1998) rather than a cosmological constant.

We thank B. Paczyński for many helpful discussions, and the anonymous referee whose comments helped to improve our results. LXL's research was supported by NASA through Chandra Postdoctoral Fellowship grant number PF1-20018 awarded by the Chandra X-ray Center, which is operated by the Smithsonian Astrophysical Observatory for NASA under contract NAS8-39073. JPO's research was supported by the NSF grants ASC-9740300 (subaward 766) and AST-9803137.

REFERENCES

Bahcall, N. et al. 2003, ApJ, 585, 182

Bahcall, N., Ostriker, J. P., Perlmutter, S., & Steinhardt, P. J. 1999, Science, 284, 1481

Bartelmann, M., & Schneider, P. 2001, Phys. Rep., 340, 291

Benson, A. J., Lacey, C. G., Baugh, C. M., Cole, S., & Frenk, C. S. 2002, MNRAS, 333, 156

Blumenthal, G. R., Faber, S. M., Flores, R., & Primack, J. R. 1986, ApJ, 301, 27

Bode, P., Ostriker, J. P., & Turok, N. 2001, ApJ, 556, 93

Borgani, S. 2001, ApJ, 561, 13

Bridle, S., Lahav, O., Ostriker, J. P., & Steinhardt, P. J. 2003, Science, 299, 1532

Browne, I. W. A. et al. 2003, MNRAS, 341, 13

Bullock, J. S. et al. 2001, MNRAS, 321, 559

Caldwell, R. R., Dave, R., & Steinhardt, P. J. 1998, Phys. Rev. Lett., 80, 1582

Cohn, J. D., Kochanek, C. S., McLeod, B. A., Keeton, C. R. 2001, ApJ, 554, 1216

Courbin, F., Saha, P., & Schechter, P. L. 2002, astro-ph/0208043

Dahle, H., Hannestad, S., & Sommer-Larsen, J. 2003, ApJ, 588, L73

Davis, A. N., Huterer, D., & Krauss, L. M. 2003, astro-ph/0210494

Efstathiou, G. et al. 2002, MNRAS, 330, L29

Eisenstein, D. J., & Hu, W. 1999, ApJ, 511, 5

Ghigna, S., Moore, B., Governato, F., Lake, G., Quinn, T., & Stadel, J. 2000, ApJ, 544, 616

Gladders, M. D. et al. 2003, astro-ph/0303341

Goodman, J. 2000, New Astronomy, 5, 103

Gott, J. R., & Gunn, J. E. 1974, ApJ, 190, L105

Helbig, P. 2000, astro-ph/0008197

Kauffmann, G., White, S. D. M., & Guiderdoni, B. 1993, MNRAS, 264, 201

Keeton, C. R. 2001, ApJ, 561, 46

Keeton, C. R., & Madau, P. 2001, ApJ, 549, L25

Li, L. -X., & Ostriker, J. P. 2002, ApJ, 566, 652 (LO02)

Ma, C. P. 2003, ApJ, 584, L1

Marlow, D. R., Rusin, D., Jackson, N., Wilkinson, P. N., & Browne, I. W. A. 2000, AJ, 119, 2629

Meyers, S. T. et al. 2003, MNRAS, 341, 1

Navarro, J. F., Frenk, C. S., & White, S. D. M. 1996, ApJ, 462, 563

Navarro, J. F., Frenk, C. S., & White, S. D. M. 1997, ApJ, 490, 493

Nemiroff, R. J., Marani, G. F., Norris, J. P., & Bonnell, J. T. 2001, Phys. Rev. Lett., 86, 580

Oguri, M., Taruya, A., & Suto, Y. 2001, ApJ, 559, 572

Oguri, M., Taruya, A., Suto, Y., & Turner, E. L. 2002, ApJ, 568, 488

Ostriker, J. P., & Steinhardt, P. J. 1995, Nature, 377, 600

Peacock, J. A. et al. 2001, Nature, 410, 169

Phillips, P. M. et al. 2001, MNRAS, 328, 1001

Porciani, C., & Madau, P. 2000, ApJ, 532, 679

Press, W. H., & Schechter, P. 1974, ApJ, 187, 425

Rees, M. J., & Ostriker, J. P. 1977, MNRAS, 179, 541

Reiprich, T. H., & Böhringer, H. 2002, ApJ, 567, 716

Ricotti, M. 2002, astro-ph/0212146

Rix, H. W., de Zeeuw, P. T., Cretton, N., van der Marel, R. P., & Carollo, C. M. 1997, ApJ, 488, 702

Romanowsky, A. J., & Kochanek, C. S. 1999, ApJ, 516, 18

Rusin, D. 2002, ApJ, 572, 705

Rusin, D., & Ma, C. P. 2001, ApJ, 549, L33

Rusin, D., & Tegmark, M. 2001, ApJ, 553, 709

Rusin, D., Kochanek, C. S., & Keeton, C. R. 2003, ApJ, in press (astro-ph/0306096)

Sand, D. J., Treu, T., & Ellis, R. S., ApJ, 574, L129

Schechter, P. 1976, ApJ, 203, 297

Schneider, P., Ehlers, J., & Falco, E. E. 1992, Gravitational Lenses (Berlin: Springer-Verlag)

Seljak, U. 2002, MNRAS, 337, 769

Somerville, R. S., Primack, J. R. 1999, MNRAS, 310, 1087

Spergel, D. N.,& Steinhardt, P. J. 2000, Phys. Rev. Lett., 84, 3760

Spergel, D. N. et al. 2003, astro-ph/0302209

Stoughton, C. et al. 2002, AJ, 123, 485

Subramanian, K., Cen, R., & Ostriker, J. P. 2000, ApJ, 538, 528

Treu, T., & Koopmans, L. V. E. 2002, ApJ, 575, 87

Turner, E. L. 1990, ApJ, 365, L43

Turner, E. L., Ostriker, J. P., & Gott, J. R. 1984, ApJ, 284, 1

Viana, P. T. P., Nichol, R. C., & Liddle, A. R. 2002, ApJ, 569, L75

Wambsganss, J., Bode, P., & Ostriker, J. P. 2003, astro-ph/0306088

Wambsganss, J., Cen, R., Ostriker, J. P., & Turner, E. L. 1995, Science, 268, 274

Wang, L., & Steinhardt, P. J. 1998, ApJ, 508, 483

Wang, L., Caldwell, R. R., Ostriker, J. P., & Steinhardt, P. J. 2000, ApJ, 530, 17

Wilkinson, P. N. et al. 2001, Phys. Rev. Lett., 86, 584

Wyithe, J. S. B., Turner, E. L., & Spergel, D. N. 2001, ApJ, 555, 504

Yamamoto, K. 2002, MNRAS, 334, 958

York, et al. 2000, AJ, 120, 1579

Zhao, H. S. 1996, MNRAS, 278, 488

This preprint was prepared with the AAS LaTeX macros v5.0.

Table 1. Cosmological Models Calculated in the Paper

Model	Ω_m	Ω_Λ	σ_8	h	n_s	Normalization
LCDM	0.27	0.73	0.84	0.7	0.96	*WMAP*[a]
LCDM2	0.19	0.81	0.9	0.7	0.96	$\sigma_8\Omega_m^{0.6} = 0.33$[b]
LCDM3	0.3	0.7	0.7	0.7	0.96	$\sigma_8\Omega_m^{0.6} = 0.33$[b]
OCDM	0.3	0	0.85	0.7	0.96	$\sigma_8\Omega_m^{\gamma} = 0.5$[c]
SCDM	1	0	0.5	0.7	0.96	$\sigma_8\Omega_m^{\gamma} = 0.5$[c]

[a]From Spergel et al. (2003).

[b]From Bahcall et al. (2003).

[c]From Wang & Steinhardt (1998) and Wang et al. (2000), $\gamma = 0.33 + 0.35\Omega_m$.

Note. — See the text for meanings of symbols.

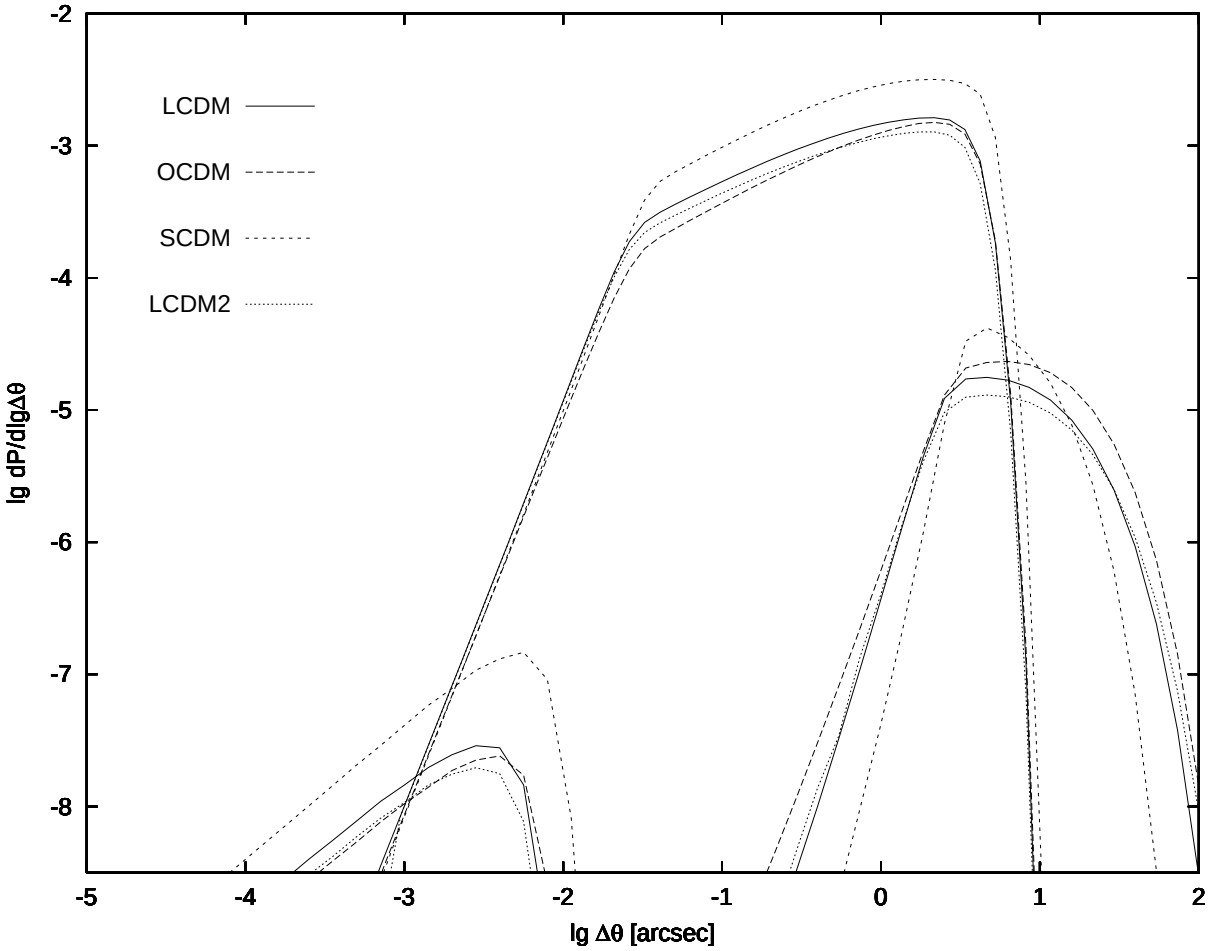

Fig. 1.— Differential lensing probability of image separation for the three components in the compound population of dark halos. Four cosmological models are shown: LCDM, OCDM, SCDM, and LCDM2 (for definitions see Table 1). The tallest islands in the middle are for Population A (galaxies). The lower islands on the right are for Population B (cluster halos). The smallest islands on the left are for Population C (dwarf halos). The source object is at $z_S = 3$.

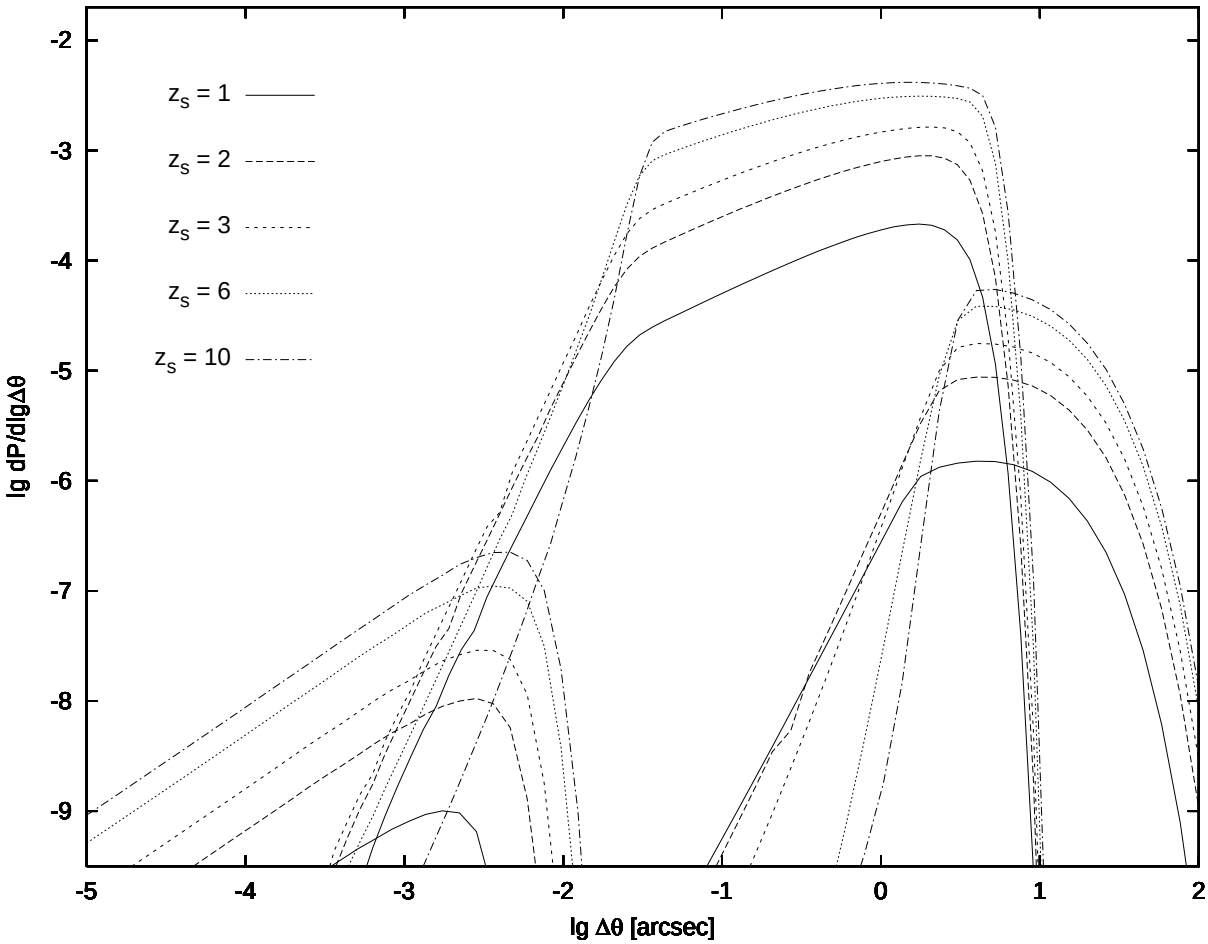

Fig. 2.— Differential lensing probability of image separation for the LCDM model. Different type of lines corresponds to different redshift of the source object as indicated in the figure. As in Fig. 1, each island in the figure corresponds to one of the three components in the compound population: Population A (center), Population B (right), and Population C (left).

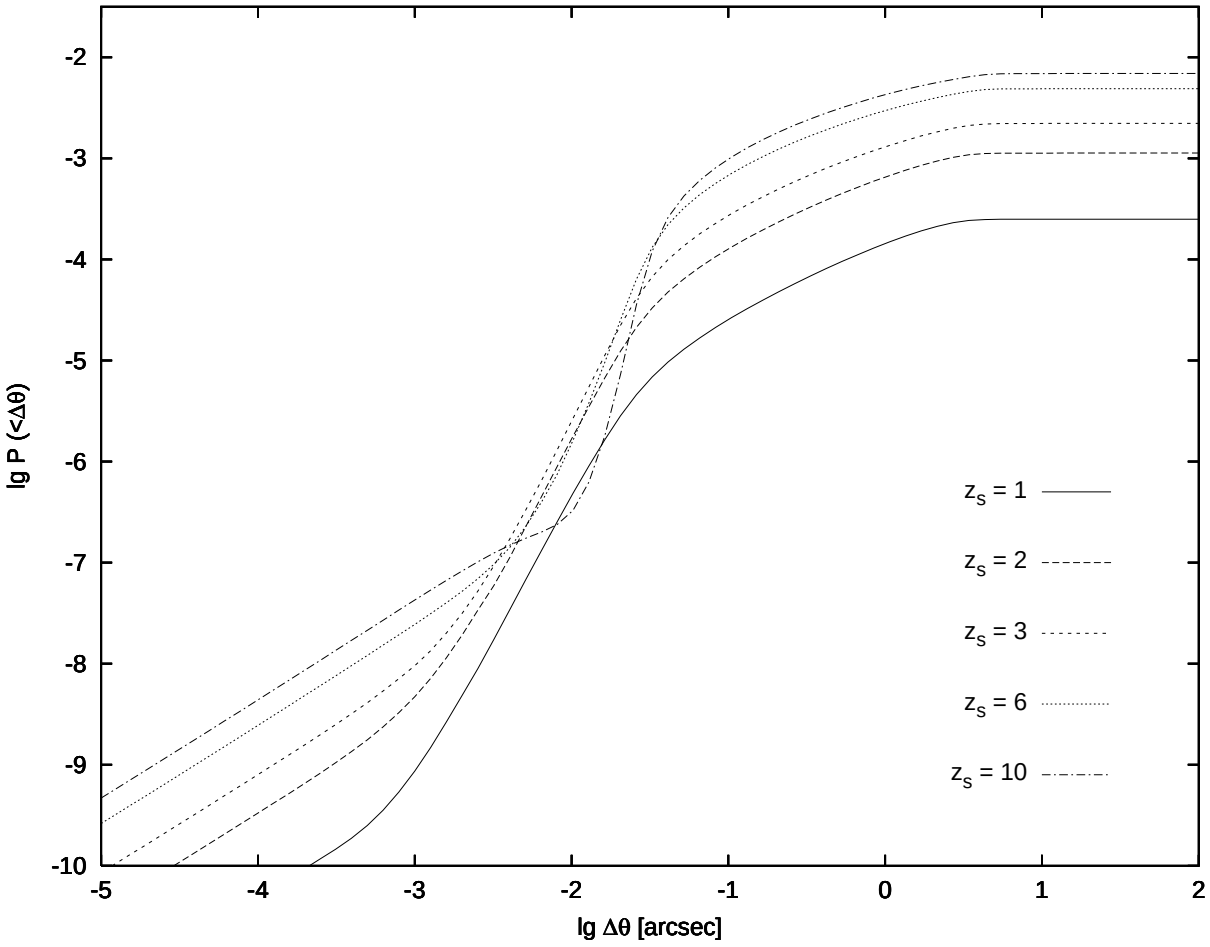

Fig. 3.— The integral lensing probability $P(< \Delta\theta)$ produced by the compound population of dark halos. The models and the meaning of symbols are the same as those in Fig. 2.

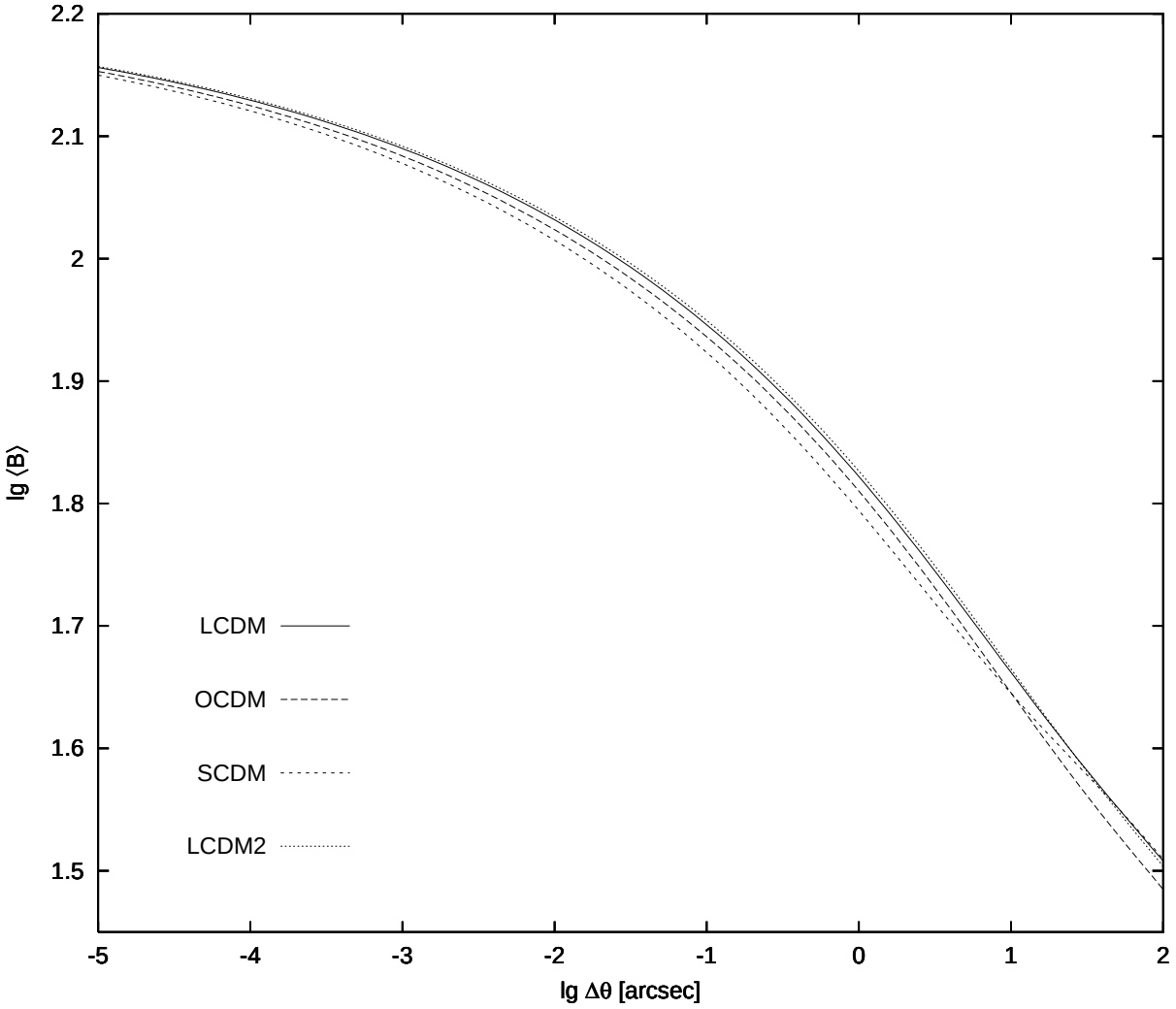

Fig. 4.— Average magnification bias as a function of image separation for GNFW lenses with $\alpha = 1.3$ and $\beta = 2.1$. The cosmological models and the meaning of symbols are the same as those in Fig. 1, except that $z_S = 1.27$ (to be consistent with the JVAS/CLASS survey). (For comparison, the corresponding magnification bias for SIS lenses is a constant $B = 4.76$.)

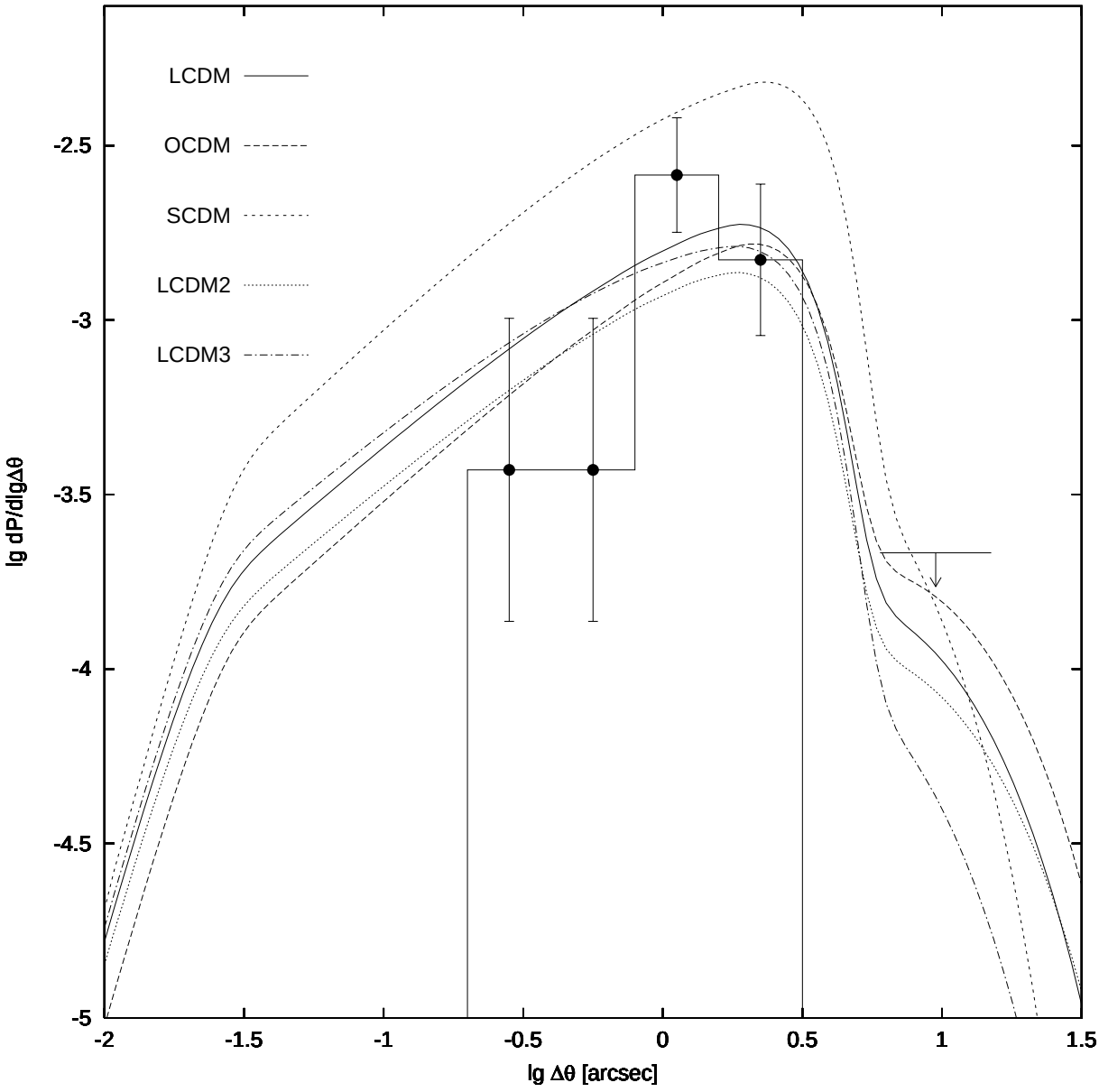

Fig. 5.— Comparison with the JVAS/CLASS data. Predictions by five different cosmological models are shown with different type of curves as indicated (see Table 1 for definitions for the cosmological models). The redshift of the source object is assumed to be $z_S = 1.27$. The data with error bars are taken from JVAS/CLASS survey (Browne et al. 2003). The null result for lenses with $6'' \leq \Delta\theta \leq 15''$ is shown with the horizontal line with a downward arrow indicating that is an upper limit.

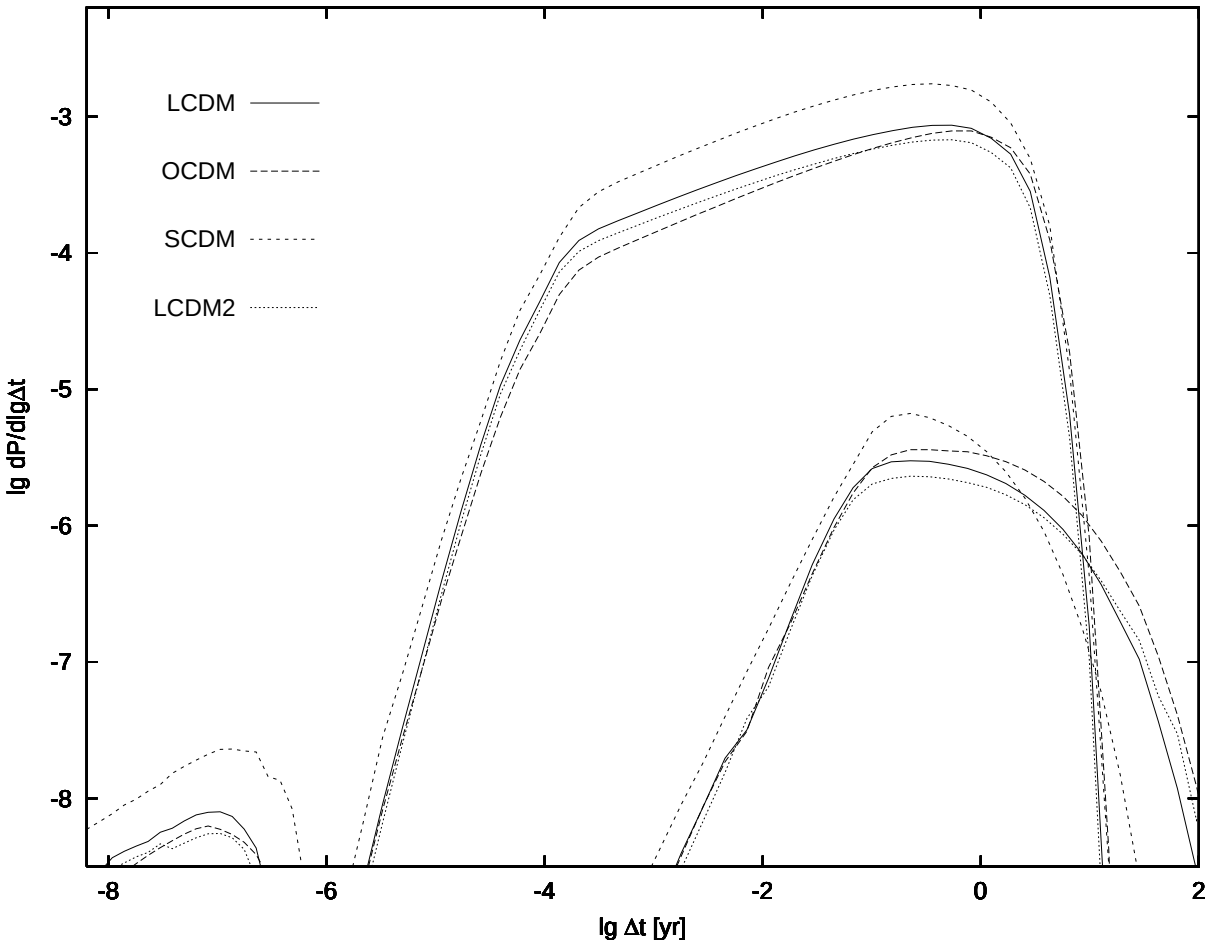

Fig. 6.— Differential lensing probability of time delay for the three components in the compound population of dark halos. The models and the meaning of the symbols are the same as those in Fig. 1. Of the studied models only SCDM can be excluded by the JVAS/CLASS observational data (see Fig. 5).

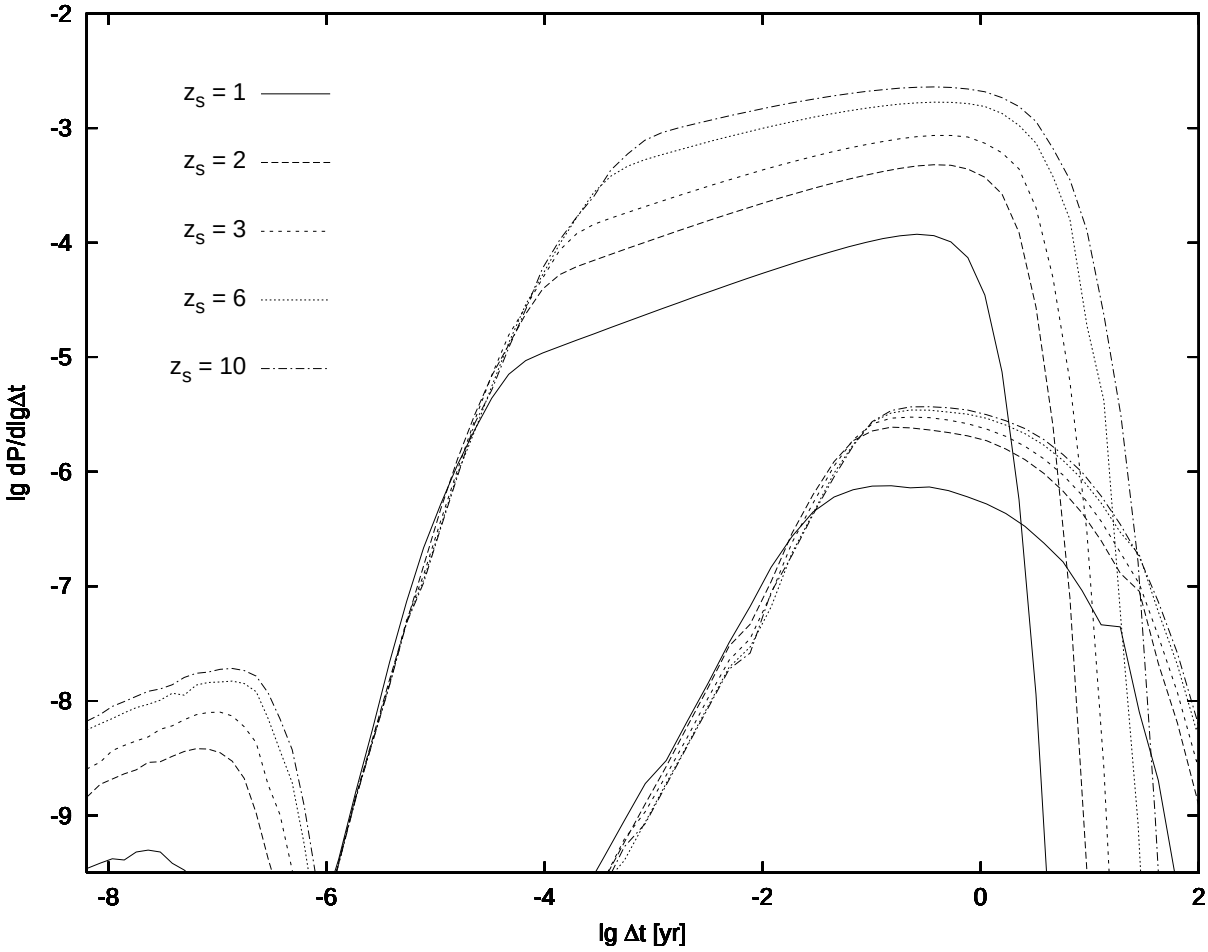

Fig. 7.— Differential lensing probability of time delay for the LCDM model corresponding to different redshift of the source object. The models and the meaning of the symbols are the same as those in Fig. 2.

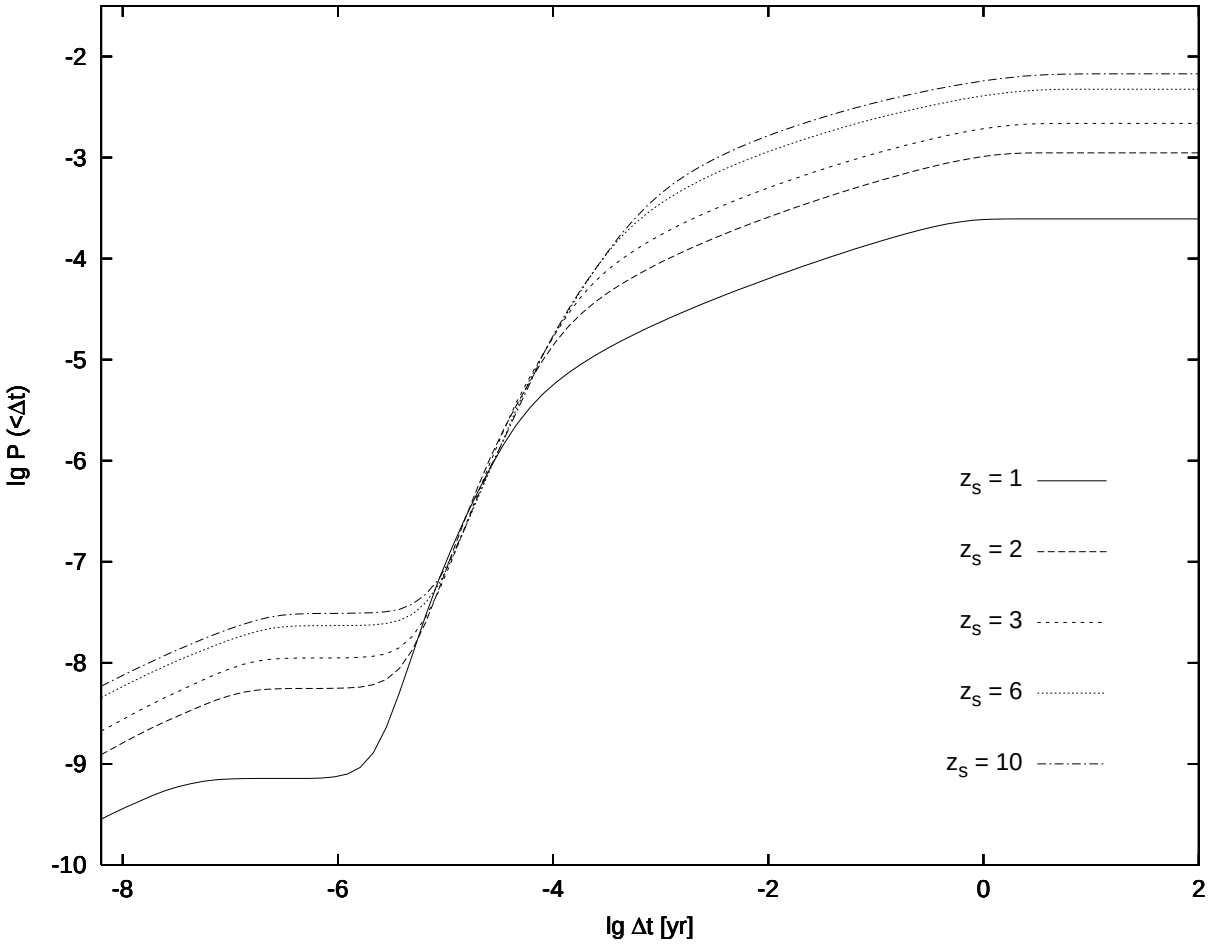

Fig. 8.— The same as Fig. 7 but for the integral lensing probability $P(< \Delta t)$.

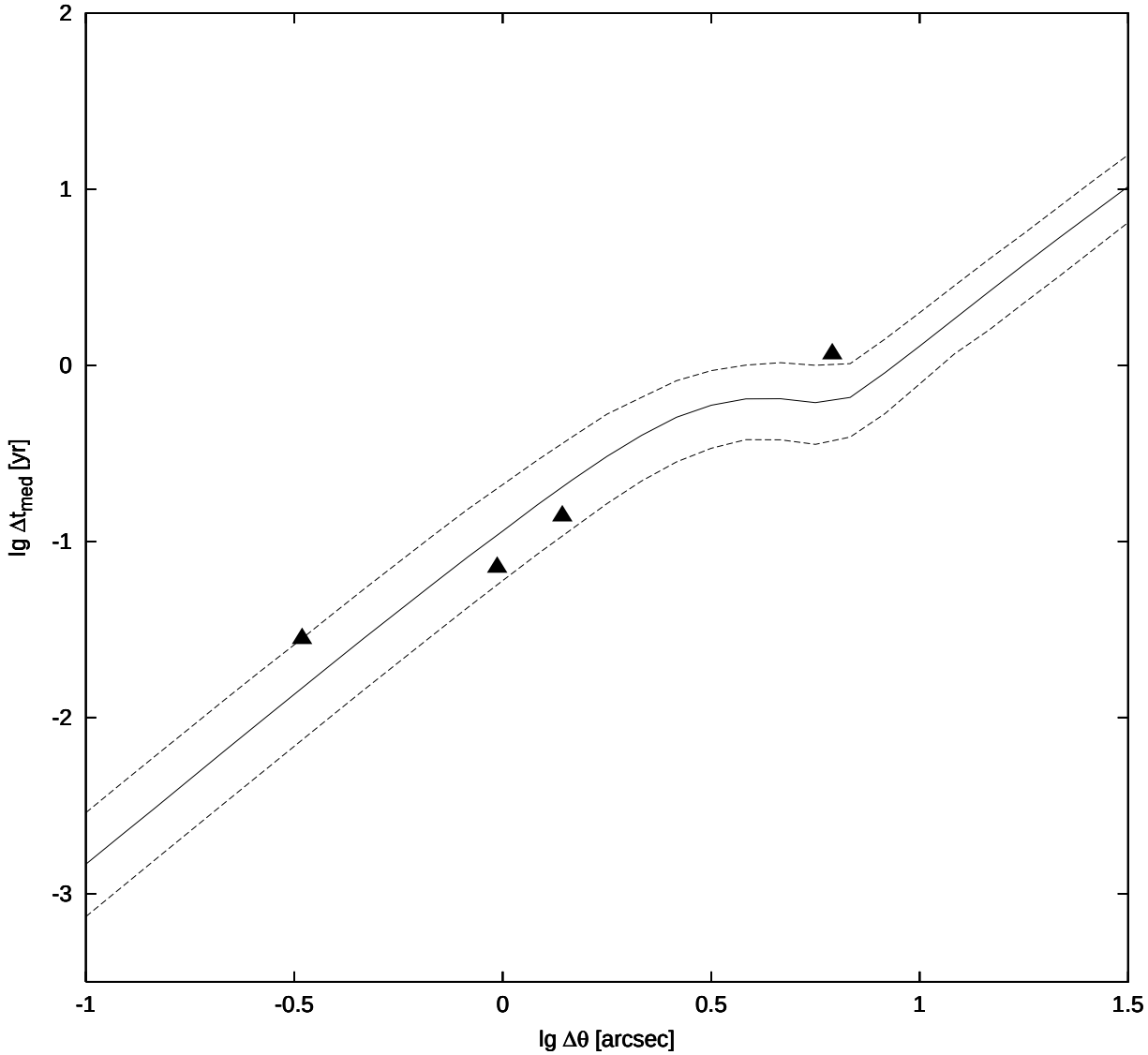

Fig. 9.— The median distribution of time delay (solid line) as a function of image separation, produced by the compound model of dark halos in the LCDM model. (The results for this figure are insensitive to the cosmological parameters.) The source object is assumed to be at $z_S = 1.27$. The dashed lines show the quadrant deviations. The observational data are taken from Oguri et al. (2002).